Relationship between the Subtropical Anticyclone and Diabatic Heating

YIMIN LIU, GUOXIONG WU, AND RONGCAI REN

State Key Laboratory of Numerical Modeling for Atmospheric Sciences and Geophysical Fluid Dynamics, Institute of Atmospheric Physics, Chinese Academy of Sciences, Beijing, China

(Manuscript received 28 October 2002, in final form 21 July 2003)

ABSTRACT

Monthly mean reanalysis data and numerical experiments based on a climate model are employed to investigate the relative impacts of different types of diabatic heating and their synthetic effects on the formation of the summertime subtropical anticyclones. Results show that the strong land surface sensible heating (SE) on the west and condensation heating (CO) on the east over each continent generate cyclones in the lower layers and anticyclones in the upper layers, whereas radiative cooling over oceans generates the lower-layer anticyclone and upper-layer cyclone circulations. Such circulation patterns are interpreted in terms of the atmospheric adaptation to diabatic heating through a potential vorticity–potential temperature view. A Sverdrup balance is used to explain the zonally asymmetric configuration of the surface subtropical anticyclones. The strong deep CO that is maximized in the upper troposphere over the eastern continent and the adjacent ocean is accompanied by upper-tropospheric equatorward flow and weaker lower-tropospheric poleward flow, whereas the very strong longwave radiative cooling (LO) that is maximized near the top of the planetary boundary layer over the eastern ocean is accompanied by strong surface equatorward flow and weaker upper-layer poleward flow. The center of the surface subtropical anticyclone is then shifted toward the eastern ocean, and its zonal asymmetry is induced. This study concludes that in the summer subtropics over each continent and its adjacent oceans LO, SE, CO, and a double-dominant heating (D) from west to east compose a LOSECOD heating quadruplet. A specific zonal asymmetric circulation pattern is then formed in response to the LOSECOD quadruplet heating. The global summer subtropical heating and circulation can then be viewed as ''mosaics'' of such quadruplet heating and circulation patterns, respectively.

1. Introduction

In winter, westerlies dominate in the midlatitudes and subtropics in the free troposphere, and mountain forcing plays an important role in the formation of the circulation patterns in these areas (Charney and Elliason 1949; Bolin 1950; Yeh 1950; Rodwell and Hoskins 2001). In the summer subtropics on the other hand, the westerlies are weak, and thermal forcing becomes more important in influencing the circulation pattern (Hoskins 1987). Webster (1972) used a two-layer linear model to show that latent heating is an important local source in maintaining the stationary circulations in low latitudes. Based on another two-layer linear model, Egger (1978) attempted to separate the contributions of sensible heating and latent heating from the maintenance of the summertime subtropical anticyclones and reached a similar conclusion. However due to the coarse vertical resolution, their models greatly underestimated the impacts of the sensible heating in the planetary boundary layer, and this conclusion needs to be reexamined.

Corresponding author address: Dr. Yimin Liu, LASG, Institute of Atmospheric Physics, Chinese Academy of Sciences, Beijing 100029, China.
E-mail: lym@lasg.iap.ac.cn

During the past several years, the impacts of monsoon condensation heating on the formation of the subtropical anticyclone have been reported on by different studies (Hoskins 1996; Liu et al. 1999b, 2001; Rodwell and Hoskins 2001). All of these results demonstrate that the surface anticyclones forced by monsoon heating alone are too weak compared to observations. In contrast, Chen et al. (2001) reported that latent heating can produce a strong surface subtropical anticyclone in a linear quasigeostrophic model. Rodwell and Hoskins (2001) used numerical experiments to show that the longwave radiative cooling (LO) over the eastern oceans significantly enhances the local descending motion and the oceanic subtropical anticyclones. Wu et al. (1999) demonstrated that the zonal advection of vorticity near the ridgeline of the subtropical anticyclone is weak and the vorticity equation can be simplified to a simple Sverdrup balance. Using this balance, Wu and Liu (2000) and Liu et al. (1999a, 2001) found that both the land surface sensible heating and deep condensation heating are important in breaking the symmetric subtropical anticyclone into isolated systems. These studies used either an individual heating or the column-integrated heating. While significant results have been obtained, many details remain unknown. For instance, the surface sub-

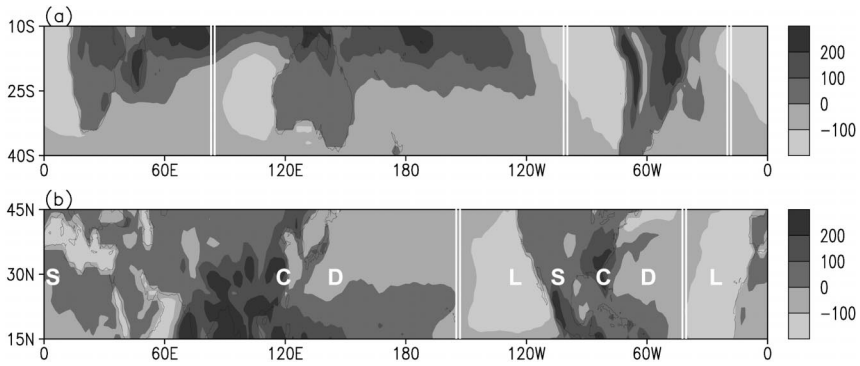

FIG. 1. Monthly mean column-integrated total heating in (a) Jan in the southern subtropics and (b) Jul in the northern subtropics. Units are W m^{-2}.

tropical anticyclones over the North Pacific and North Atlantic appear as ''triangular shaped,'' and their centers are biased to the east. Chen et al. (2001) interpreted such a ''tilting'' as a result of the meridional shear of the zonal wind. However the simulated anticyclone following this line was presented as a parallelogram with its center biased westward, quite unlike the observations. All of these imply that the synthetic diabatic effects on the maintenance of the summertime subtropical anticyclone are still unclear.

In this study, the reanalysis of the National Centers for Environment Prediction–National Center for Atmospheric Research (NCEP–NCAR; Kalnay et al. 1996) from 1980 to 1997 and a climate model are employed to investigate the separated and synthetic impacts of different thermal forcings on the formation of the summertime subtropical anticyclones. The diabatic heating in the reanalysis is not an observation, but the product of a GCM that depends on physical parameterization schemes (Newman et al. 2000). Comparisons between the NCEP heating and Q1 from European Centre for Medium-Range Weather Forecasts (ECMWF) data (Nigam et al. 2000; Rodwell and Hoskins 2001) and Tropical Ocean Global Atmosphere (TOGA) data (Lin and Johnson 1996) show that both the horizontal distribution of the column-integrated heating and the vertical heating profile are similar. Duan (2003, personal communication) also made comparisons between the NCEP–NCAR reanalysis and two other datasets. One is for observations from July 1993 to March 1999 from six Automatic Weather Stations (AWSs) over the Tibetan Plateau (Li et al. 2001). The other is the Global Energy and Water Cycle Experiment (GEWEX) Asian Monsoon Experiment (GAME) Intesive Observing Period (IOP) reanalysis from 1 April to 31 October 1998 completed by the Japan Meteorological Research Institute and the Japan Meteorological Agency (unpublished). Results show that the surface sensible heat flux and latent heat flux provided by NCEP–NCAR agree with the AWS data, and there is no significant difference in the variation and magnitude between the NCEP–NCAR and GAME-IOP daily datasets. This then validates the usage of the NCEP–NCAR reanalysis for the present study, although caution is required since both the AWS and GAME-IOP data have limited spatial and temporal coverage. Section 2 shows the observed distributions of the subtropical circulation against diabatic heating in July for the Northern Hemisphere and in January for the Southern Hemisphere. In section 3, the relevant dynamics concerning the atmospheric responses to different kinds of heating are reviewed briefly, and the factors in generating the zonally asymmetric subtropical anticyclones are explored. Numerical experiments are then designed in section 4 to compare with observations and to verify the hypothesis presented in section 3. In section 5, all of these different kinds of forcings are put together to get their synthetic impacts on the formation of the summertime subtropical anticyclone. Conclusions and discussion are presented in section 6.

2. Diabatic heating and circulation in summer subtropics

a. Column-integrated total heating and surface sensible heating

The distributions of the column-integrated total diabatic heating (TH) retrieved from the NCEP–NCAR reanalysis for January and July are presented in Fig. 1. Along the summer subtropics, except in lower latitudes, heating is usually over land and cooling is over ocean. The distributions of the zonal deviation of geopotential height at different levels are shown in Fig. 2. In both the Southern and Northern Hemispheres, the surface lows are located over the subtropical continents, with strong equatorward flow existing along, and to the west of, the western coastal regions (Figs. 2b and 2d), whereas the surface subtropical anticyclone centers are located in the eastern parts of the oceans, with magnitudes of more than 30 gpm in the Southern Hemisphere and 90 gpm in the Northern Hemisphere. At 200 hPa (Figs. 2a and 2c), the subtropical anticyclones are observed over continents, whereas troughs are located over oceans. The magnitude of the anticyclones in the Southern

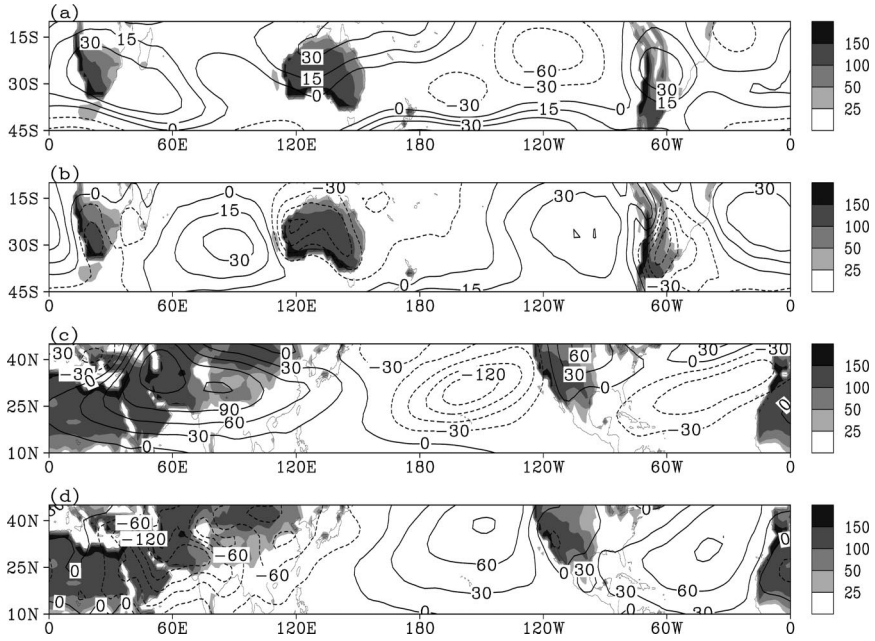

FIG. 2. Monthly mean distributions of the zonal deviation of the geopotential height (units are gpm) and of sensible heat flux at the surface (shading, units are W m^{-2}) at (a), (c) 200 and (b), (d) 1000 hPa, for (a), (b) Jan and (c), (d) Jul.

Hemisphere is more than 30 gpm. The North American high is more than 60 gpm, whereas the South Asian high is stronger than 120 gpm and spans a vast longitudinal domain in the subtropics ranging from North Africa to the western Pacific. It is more than twice as strong as its counterpart over North America. Comparing Fig. 2 to Fig. 1, a prominent feature is then obtained: the positive TH over each subtropical continent in the summer hemisphere is accompanied by the surface cyclone and the upper-layer anticyclones, whereas the negative TH over each subtropical ocean sector is accompanied by the surface anticyclone and the upper-layer cyclonic circulation. Such a coordination between TH and the circulation pattern can be well understood by using the potential vorticity–potential temperature (PV–θ) view proposed by Hoskins (1991); namely, heating (cooling) generates lower-layer cyclonic (anticyclonic) circulation and upper-layer anticyclonic (cyclonic) circulation. Therefore, as a first approximation, the summer subtropical circulation as presented in Fig. 2 can be interpreted as the adaptation of atmospheric circulation to the diabatic heating (Wu and Liu 2000) along the subtropics.

The distributions along summer subtropics of the surface sensible heat flux are also shown in Fig. 2. In January in the Southern Hemisphere (Figs. 2a and 2b), it is more than 100 W m^{-2} over Australia, and over the western coasts of South Africa and South America. In July in the northern subtropics (Figs. 2c and 2d), the area of more than 100 W m^{-2} covers western North America, North Africa, and western and middle Asia. A prominent feature is then obtained: strong surface sensible heating (SE) exists over each subtropical continent in the summer hemisphere, particularly over the western coasts. Comparing Fig. 2 with Fig. 1, we see that except for the eastern part, the positive TH over the western and central parts of each continent in the summer subtropics mainly result from the in situ SE. In addition, the centers of either the surface cyclones or the upper-layer anticyclones over continents are located over the SE areas. All of these imply the significance of the continental SE in the maintenance of the summertime subtropical circulations.

b. Deep condensation heating (CO)

The distributions in summer months of deep condensation heating (CO) and the associated zonal deviation winds in the upper and lower troposphere are presented in Fig. 3. In January (Figs. 3a and 3b), the three subtropical heating regions are located, respectively, from eastern Africa to about 80°E, from eastern Australia to 120°W, and from the eastern coast of Brazil to 25°W. Strong CO along the western coast of South America is also observed due to the Andes. At 850 hPa (Fig. 3b), poleward flow dominates the region of convective heating except along the eastern coast of Australia where weak equatorward flows exist due to the local orographic forcing. The strong CO centers of more than 250 W m^{-2} over Madagascar and along the eastern coast of Brazil in the subtropics and over the eastern side of the date line in the Tropics are all accompanied by poleward flows of more than 4 m s^{-1}. Apparent subtropical cyclone and anticyclone circulations are therefore ob-

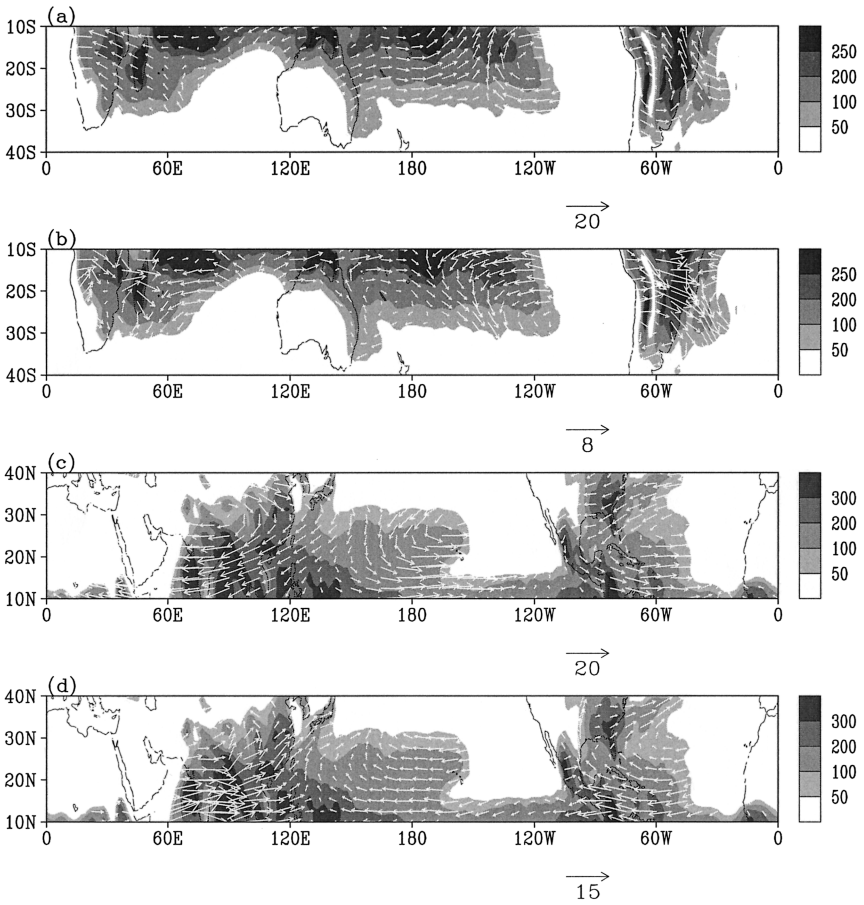

FIG. 3. Monthly mean distributions of the zonal deviation wind (vector; units are m s^{-1}) and of convective condensation heating (shading; units are W m^{-2}) at (a), (c) 200 and (b), (d) 850 hPa, for (a), (b) Jan and (c), (d) Jul.

served, respectively, to the west and east of these strong CO centers. In the upper troposphere (Fig. 3a), equatorward flow prevails over these regions of deep condensation heating in the subtropics, and anticyclonic and cyclonic circulations are observed, respectively, to the west and east of these heating centers.

In July (Figs. 3c and 3d), CO of more than 50 W m^{-2} also exists over areas from the eastern continents to the western oceans along the subtropics. While the area of more than 100 W m^{-2} over the western Atlantic is more confined to the coastal region, it appears over the whole western Pacific and extends beyond the date line. Strong CO of more than 250 W m^{-2} is observed over the southeastern continental United States and eastern China. As in the Southern Hemisphere, equatorward flow in the upper troposphere (Fig. 3c) and poleward flow in the lower troposphere (Fig. 3d) prevail over these two strong heating areas. The flows are more pronounced and organized particularly over the Asian monsoon area. As a result, prominent anticyclone circulations are found to the west of the strong CO regions in the upper troposphere, and to their east in the lower troposphere.

c. Radiative cooling

The distributions in summer months of the column-integrated cooling (copied from Fig. 1) and the associated zonal deviation winds in the upper and lower troposphere are presented in Fig. 4. Cooling covers the eastern oceans and the poleward side of the western oceans in the subtropics. In particular, it is stronger than -100 W m^{-2} over the eastern coastal region of each ocean basin. The zonal deviation circulations, in association with such cooling, bear common features over each of the five subtropical ocean basins; namely, the surface anticyclonic and upper-layer cyclonic circulations appear in the cooling region over oceans, as discussed in section 2a and emphasized by Rodwell and Hoskins (2001). Another remarkable feature revealed in Fig. 4 is that strong surface equatorward flow and upper-layer poleward flow appear over the eastern offshore ocean region where radiative cooling becomes the main feature of the atmospheric heating. Such a relationship between the meridional flow and radiative cooling can also be detected over the Mediterranean Sea. The only exception is observed along the western coastal region

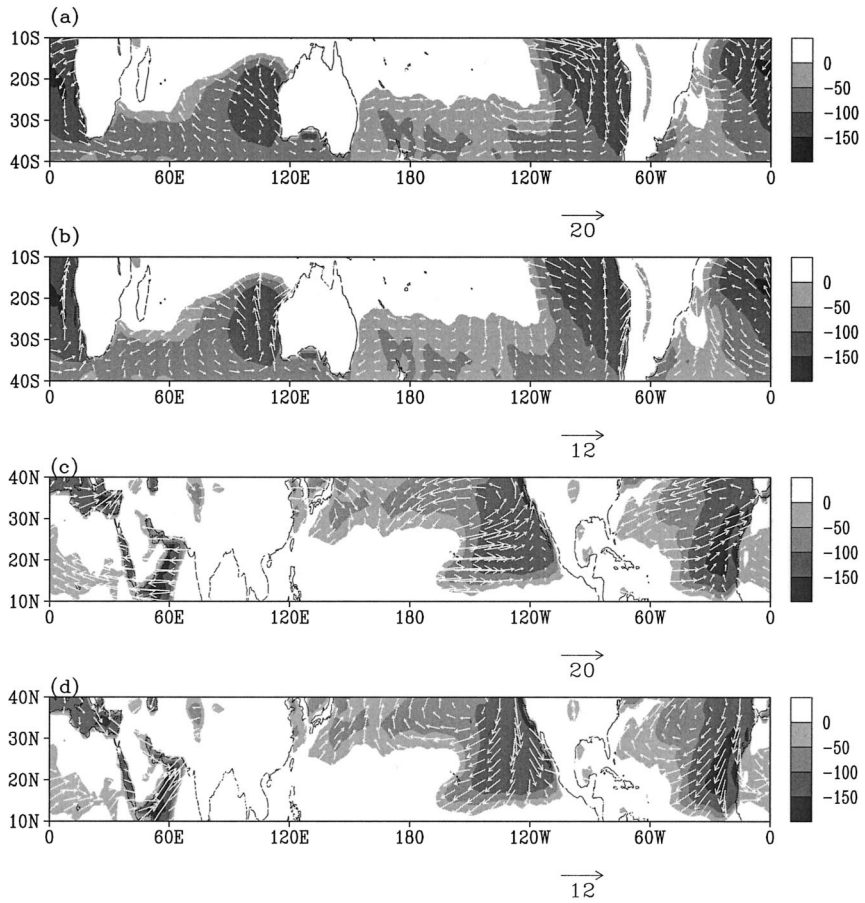

FIG. 4. Monthly mean distributions of the zonal deviation wind (vector; units are m s^{-1}), and of column-integrated cooling (shading; units are W m^{-2}) at (a), (c) 200 and (b), (d) 1000 hPa, for (a), (b) Jan and (c), (d) Jul.

of the Arabian Sea, where southerlies develop in the lower troposphere due to the strong suction of the elevated heating over the Tibetan Plateau in summer (Wu et al. 1997a; Ye and Wu 1998).

3. Dynamics relevant to the maintenance of the subtropical anticyclone

Although the theory of the thermal adaptation of atmospheric circulation to diabatic heating presented above can be used to explain the general distributions of the summertime subtropical anticyclone, it cannot explain the asymmetric configurations of the subtropical anticyclone in several detailed aspects. For instance, strong meridional flows either in the upper or in the lower troposphere along the subtropics are usually associated with strong condensation heating (Fig. 3) or radiative cooling (Fig. 4); the equatorward flow in the region along, and to the west of, the western coast of each continent near the earth's surface is much developed; and the center of the surface anticyclone over ocean is biased eastward (Fig. 2), etc. All these cannot be simply explained by the thermal adaptation theory. A theoretical study by Gill (1980) shows that the atmospheric response to a heating source or sink located in low latitudes exhibits an asymmetric Rossby wave pattern. In the Northern Hemisphere, southwesterlies (northeasterlies) are generated to the east of the heating source (sink). Although this theory can be used to interpret the tilting of the subtropical anticyclones, it cannot explain the eastward bias of the surface subtropical anticyclone centers.

To help understand these asymmetries, based on the NCEP–NCAR reanalysis, the July mean heating profiles at different locations along the ridgeline of the subtropical anticyclone in the Northern Hemisphere are present in Fig. 5. Those in the southern subtropics are similar and are not shown here. To confirm the dominance of different types of heating in different locations, the vertical profiles of CO, SE, LO, and TH (including other types of heating) at typical sites are presented. Figure 5a is for the area based in the Western Hemisphere, whereas Fig. 5b is for the area based in the Eastern Hemisphere. The four sites L (30°N, 122°W), S (30°N, 108°W), C (30°N, 80°W), and D (30°N, 60°W) selected for plotting in Fig. 5a and the four sites L (30°N, 24°W),

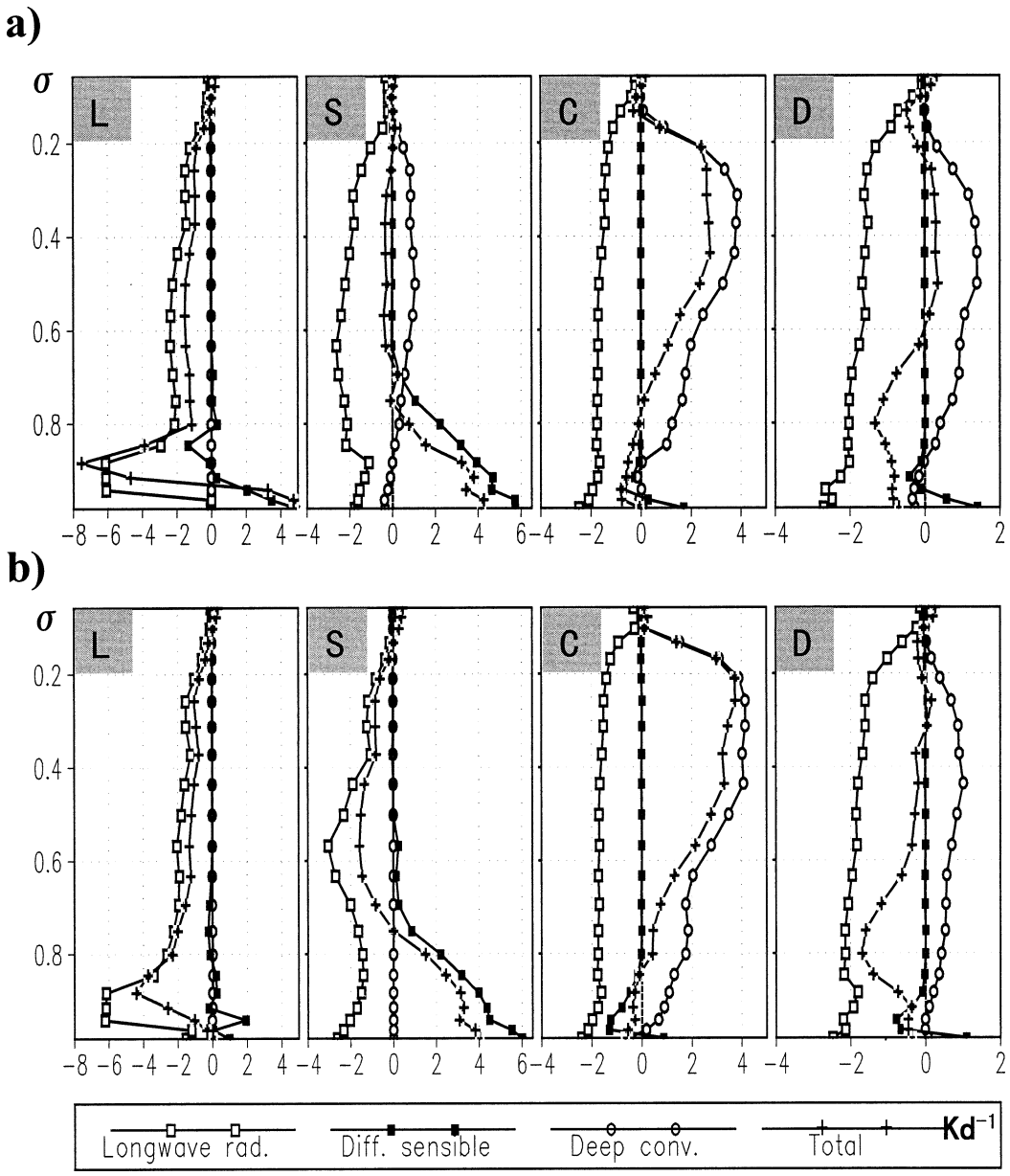

FIG. 5. Vertical profiles of various Jul mean heating at sites L, S, C, and D as indicated in Figs. 1b and 13 in the (a) western and (b) eastern Northern Hemisphere. Shown are longwave radiative cooling (LO, open square), diffusive sensible heating (SE, filed square), deep condensation heating (CO, open circle), and total heating (TH, cross, including all other heating). Units are K day^{-1}.

S (30°N, 0°), C (30°N, 120°E), and D (30°N, 145°E) selected for plotting in Fig. 5b are located, respectively, within different heating lobes as marked in Fig. 1b (and also in Fig. 13).

At the L sites (left panels) over the eastern Pacific and Atlantic, weak SE is near the surface, and no apparent CO is observed. Strong LO values of −6.5 K day^{-1} over the eastern Pacific and Atlantic appear in the lower layer between 0.5 and 1.5 km ($\sigma \sim 0.85$ and 0.95) above sea level. The profile of TH then follows the LO profile. These regions are therefore defined as the LO heating lobes. At the S sites (middle-left panels) over western North America (Fig. 5a) and North Africa (Fig. 5b), CO is weak, and SE dominates the lower troposphere with a maximum of about 6 K day^{-1} near the surface. The TH profile in these areas then follows the SE profile. These regions are therefore defined as the SE heating lobes. At the C sites (middle-right panels) along the eastern coasts of North America (Fig. 5a) and China (Fig. 5b), the thick CO with a maximum of about 4 K day^{-1} in the upper troposphere is the main feature, and the TH profile follows the CO profile. These regions

are therefore defined as the CO heating lobes. At the D sites (right panels) over the western Atlantic (Fig. 5a) and western Pacific (Fig. 5b), CO is less than 2 K day^{-1}. The CO together with other types of heating (figure not shown) exceed the longwave radiative cooling in the layer between $\sigma = 0.2$ and 0.6 over the western Atlantic and are near $\sigma = 0.2$ over the eastern Pacific, but are weaker than the cooling above and below these layers. Thus the in situ column-integrated TH is negative as shown in Fig. 1, and the TH profile in these regions is determined mainly by the double-dominant heating (D), that is, LO and CO. These regions are therefore defined as the D heating lobes. The negative TH in lobe D contributes to the occurrence of the lower- (upper-) layer anticyclonic (cyclonic) circulation and distinguishes it from lobe CO, whereas the existence of the secondary dominant heating CO in this lobe results in the development of the lower- (upper-) layer poleward (equatorward) flow wet climate and distinguishes the lobe from the LO lobe in which the climate is rather dry.

Results from Fig. 5 show that the TH profiles vary from one location to the other, and follow the profiles of LO at L, SE at S, CO at C, and the double-dominant heating at D, respectively. They compose a LOSECOD heating quadruplet over each continent and its adjacent oceans (Wu and Liu 2003).

Let us now consider how the vertical differential heating can influence the atmospheric circulations. In the subtropics, particularly along the ridgeline of the subtropical anticyclone, both the vorticity advection and transient processes are weak (Wu et al. 1999; Rodwell and Hoskins 2001; Liu et al. 2001), and vorticity equation can be simplified to the Sverdrup balance:

$$\beta v \approx \theta_z^{-1}(f + \zeta)Q_z \ (\theta_z \neq 0). \tag{1}$$

This implies that in the absence of horizontal advection and at a steady state, the increase (decrease) of the relative vorticity due to the vertical differential heating should be compensated for by the planetary vorticity (Q_z) advection brought in through the meridional winds from low (high) latitudes. Therefore *the thermally forced circulation along the subtropics depends strongly on the vertical profile of the heating.* Since f is positive in the Northern Hemisphere but negative in the Southern Hemisphere, in a statically stable atmosphere ($\theta_z > 0$) a heating that increases with altitude will generate poleward flow, whereas a heating that decreases with altitude will produce equatorward flow. This then provides another base for understanding the formation of the asymmetric configuration of the summertime subtropical anticyclone, and can be summarized below by the schematic diagrams presented in Fig. 6.

a. Surface sensible heating

During summer along the subtropics, the land surface sensible heat flux over the western continents usually exceeds 100 W m^{-2}, which amounts to a heating rate

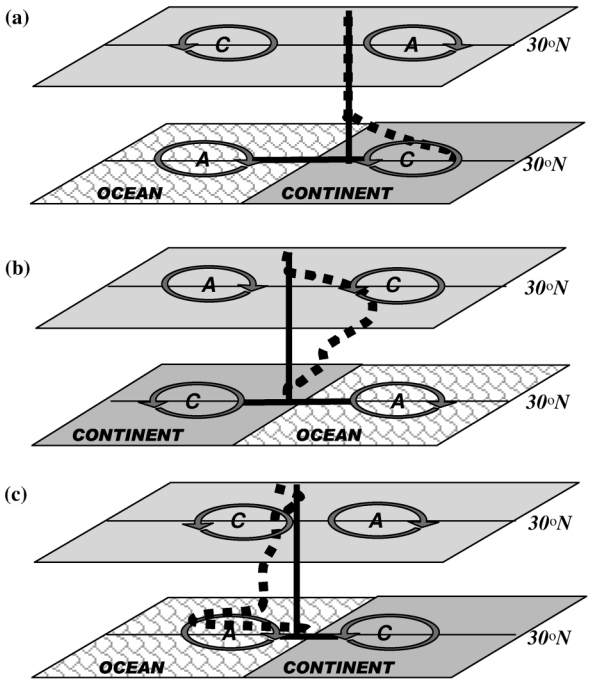

FIG. 6. Schematic diagram indicating the summertime subtropical atmospheric response to the vertically differential diabatic forcing of (a) sensible heating, (b) deep condensation heating, and (c) longwave radiative cooling. Here, A denotes an anticyclone, C denotes a cyclone, and the profiles at the centers of each panel indicate the dominating heating.

(Q) of 10^{-5} K s^{-1}. For a large-scale atmospheric system such as the subtropical anticyclone, the order of magnitude for θ_z is estimated as $O(\theta_z) \sim 10^{-2}$ K m^{-1}, and that for the forcing term on the right-hand side of (1) is estimated as 10^{-10} s^{-2}. Then the forced equatorward flow in the lower layers is estimated as 1–10 m s^{-1}. This means that, in response to a surface sensible heat flux of 100 W m^{-2}, the equatorward winds of several meters per second will be forced over the heating region in the lower layers with a thickness of about 1 km (Fig. 6a). Therefore equatorward flow on the western side of the surface cyclone should be stronger than the poleward flow on its eastern side, resulting in the westward bias of the cyclone center over the continent (Fig. 2). The intensified equatorward flow along the western coast of the continent brings colder air and favors the enhancement of sensible heat release from the warm land surface. This then explains why the strongest sensible heating in the summer subtropics appears along the western coast of each continent (Fig. 2).

b. Deep convective condensation heating

Along the subtropics, maximum CO usually occurs at a height ($z = Z_M$) between 300 and 400 hPa where the heating rate can be several degrees per day. This, following the thermal wind balance, results in a strong westerly to its north and an easterly to its south above

TABLE 1. Experiments of different external forcings (see text for detailed description).

GCM expts		Perpetual Jul experiments	
SH-1	SE alone	SH-0P	Idealized SH in an aquaplanet
SH-2	SE+LO	LH-0P	Idealized CO in an aquaplantet
CON	SE+LO+CO + orography	LH-1P	CO+LO in an aquaplanet
		LH-2P	CO+LO+orography
		SH-2P	SE+LO+orography
		CON-P	SE+LO+CO+orography

the heating region. Thus, even in the upper troposphere in the subtropics, vorticity advection above a deep convection area is usually small. By using (1), the diabatic term $\theta_z^{-1}(f + \zeta)Q_z$ is estimated to be $+10^{-10}$ s^{-2} below Z_M, but -10^{-9} s^{-2} above this level. Therefore a poleward flow of several meters per second is forced below Z_M, while a slightly stronger equatorward flow is forced in the upper troposphere. Such a mechanism then explains why in Fig. 3 the equatorward flow in the upper troposphere and the poleward flow in the lower troposphere are in accordance with the strong deep condensation heating in the subtropics. These forced strong meridional winds then contribute toward strengthening the formation of the subtropical anticyclone to the west of the deep convection region in the upper troposphere, and to its east in the lower troposphere, as schematically shown in Fig. 6b and observed in Fig. 3.

c. Longwave radiative cooling

The maximum LO is usually below 850 hPa with an intensity of about -6 K day^{-1}. Following a similar argument, such radiative cooling can produce a vorticity forcing of $+10^{-10}$ s^{-2} in the upper troposphere and -10^{-9} s^{-2} in the lower troposphere. Poleward flow of several meters per second in the upper layer and stronger equatorward flow in the lower troposphere are then forced. Such radiation-induced meridional flows reinforce those circulation patterns generated by sensible heating (Fig. 6a) and favor the formation of the subtropical anticyclone to the west of the radiative cooling in the lower troposphere, but to its east in the upper troposphere, as shown in Fig. 6c. We may therefore propose that the strong negative vorticity forcing near the surface due to LO over the eastern oceans contributes to the eastward shift of the surface oceanic subtropical anticyclone, resulting in the asymmetric configuration of the surface subtropical anticyclones over oceans.

4. Numerical experiments

To verify further the atmospheric response to external thermal forcing, numerical experiments are designed by employing the Global Ocean–Atmosphere–Land System (GOALS) model developed at the Institute of Atmospheric Physics/State Key Laboratory of Numerical Modeling for Atmospheric Sciences and Geophysical Fluid Dynamics (IAP/LASG; Wu et al. 1997b; Zhang et al. 2000; Table 1). Its atmospheric component is a spectral general circulation model that possesses nine vertical levels in σ coordinates and is rhomboidally truncated at wavenumber 15 in the horizontal. The oceanic component is a gridpoint model with horizontal resolution of 4° latitude × 5° longitude and 20 vertical layers (Zhang et al. 1996). The land surface processes are represented by the Simplified Simple Biosphere (SSiB) model (Xue et al. 1991), which has been implemented in the atmospheric component (Liu and Wu 1997). The GOALS climate model can simulate the mean climate reasonably well and has been used in climate studies for different purposes (Houghton et al. 2001; Kang et al. 2002).

In this study the ocean component of the model is switched off, and the required sea surface temperature (SST) and sea ice are prescribed by using the climate mean observation data of 1979–88 developed for the Atmospheric Model Intercomparison Project (AMIP). Because the adjustment period measured by the global surface energy balance is about half a year for each experiment, all the experiments in this section are integrated for 12 model years, and the July means calculated from the last 10 years are taken for comparisons. The normal integration is defined as a control run (CON) as shown in Table 1. A pair of GCM experiments (SH-1 and SH-2) is designed to study the contributions of sensible heating and radiative cooling to the formation of the summertime subtropical anticyclones. Another group of sensitivity runs is also designed for the boreal summer as perpetual July experiments. In these runs, the solar zenith angle is fixed at the value corresponding to 15 July, the SST assumes its zonal means, and the initial fields are taken from the July mean zonal states of the multiyear integration of the GOALS model. All the experiments are integrated for 24 months, and the results from the last 12 months are extracted for analysis. To show the responses of the atmospheric circulation to a prescribed heating, only those zonal deviation fields are plotted. All the perpetual July experiments designed for the present study are also presented in Table 1 and are described in detail in the following corresponding sections.

The distributions in CON of the July means are demonstrated in Fig. 7. The simulated distribution of the surface sensible heat flux (shading) agrees in general with that of the NCEP–NCAR reanalysis (Figs. 2c and

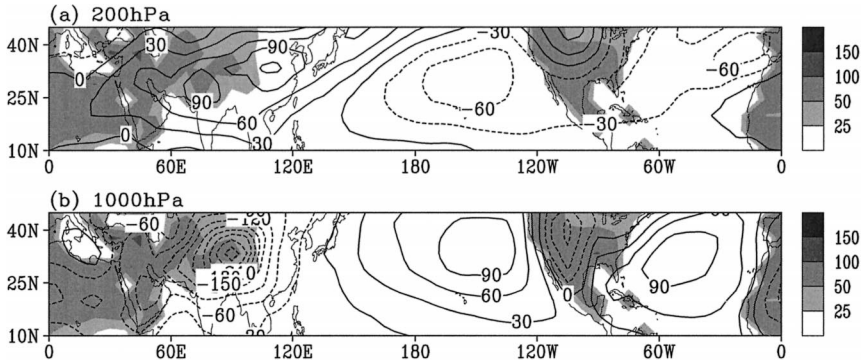

FIG. 7. Jul mean distributions in CON of the zonal deviation of geopotential height (units are gpm) and of the surface sensible heat flux (shading; units are W m^{-2}) at (a) 200 and (b) 1000 hPa.

2d), although the magnitude over eastern North America is too high. Surface cyclones and upper-layer anticyclones are produced over continents, whereas surface anticyclones and upper-layer cyclones are located over oceans. Despite the coarse resolution of the model, it is able to produce the large-scale features of the subtropical circulations.

a. Idealized thermal forcing

1) SURFACE SENSIBLE HEATING

Perpetual July and an aquaplanet are assumed for the experiment. To mimic the SE distributions over North America and over North Africa and the subtropical Asia, surface sensible heating is imposed in the two regions from 0° to 105°E and from 90° to 120°W, and between 24.4° and 46.6°N, with a heating maximum of 150 W m^{-2} located along the western boundaries and decreasing in sinusoidal form to zero along the eastern boundaries, as depicted in Fig. 8c. The cloud distribution is prescribed as zonal symmetric and is obtained from CON. The model-induced condensation heating and sensible heating are eliminated from the thermodynamic equation and are not allowed to warm the atmosphere. This experiment is labeled SH-0P. Figure 8 shows that such SE produces anticyclone highs of 50 gpm at 500 hPa (Fig. 8a) and strong surface lows of 80–100 gpm over the two heating regions (Fig. 8b). The two lows at 500 hPa and the two surface highs of more than 40 gpm are generated over the two ''oceans'' between the two heating areas. The vertical cross section along 30°N (Fig. 8c) shows that the main atmospheric response over the heating region is the generation of cyclone circulation below 700 hPa and anticyclone circulation above it, as

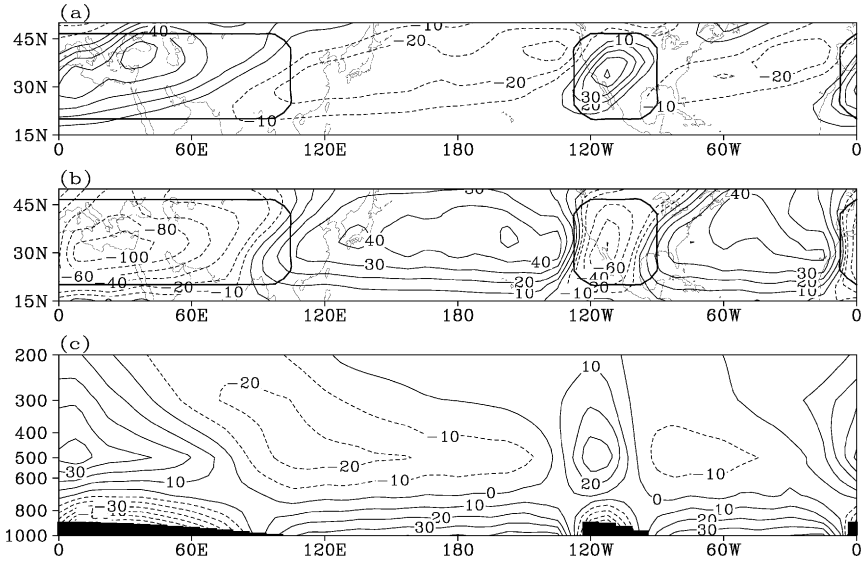

FIG. 8. Zonal deviation of geopotential height (units are gpm) at (a) 500 and (b) 1000 hPa, and (c) its vertical cross section at 30°N in the idealized perpetual Jul experiment SH-0P. The heavy curves in (a) and (b) bound the region where the heating is more than 1 W m^{-2}. Shading in (c) indicates the surface sensible heating region.

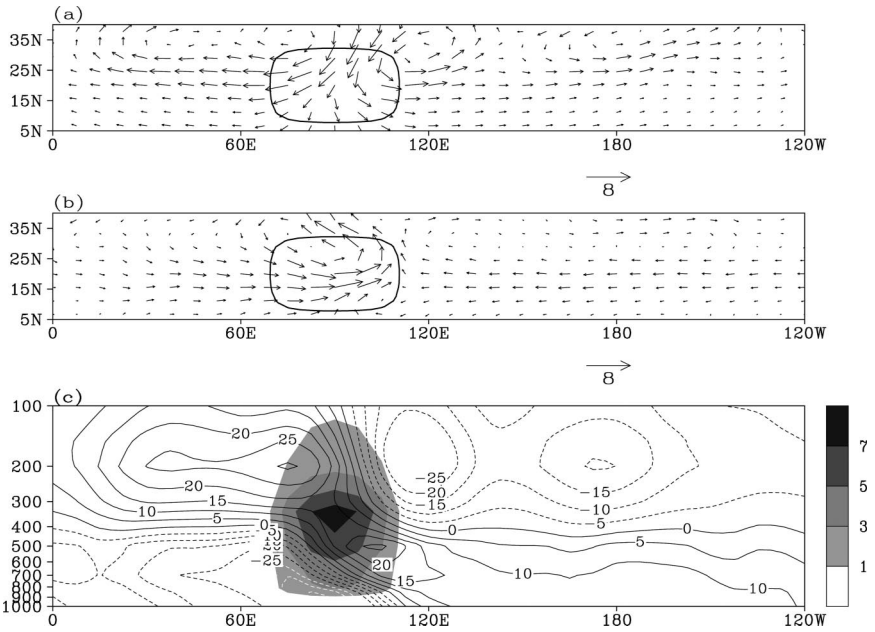

FIG. 9. Zonal deviation of horizontal wind (units are m s^{-1}) at (a) 200 and (b) 850 hPa, and (c) the vertical cross section of the geopotential height at 30°N (units are gpm) in the idealized perpetual Jul experiment LH-0P. The heavy curves bound the region where the heating is more than 1 K day^{-1} at $\sigma = 0.336$. Shading indicates the vertical profile of the heating (units are K day^{-1}).

is anticipated from the thermal adaptation theory. In lower layers, strong northeries are generated over the western heating region (Fig. 8b). It is important to note that with the imposed surface sensible heating alone, the generated pattern of geopotential height deviation at 1000 hPa already captures the main features in the observation (Fig. 2d). This implies the importance of land surface sensible heating in the formation of the subtropical anticyclone in summer at least in the lower layers.

2) DEEP CONVECTIVE CONDENSATION HEATING

The strongest convective heating in July is observed over the northern Bay of Bengal. Following the NCEP–NCAR reanalysis, a localized deep convective condensation heating is prescribed over a region from 6.7° to 33.3°N and from 67.5° to 112.5°E in an aquaplanet. A maximum heating center of 8 K day^{-1} is located at 20°N, 90°E where the basic zonal flow U vanishes at the height $\sigma = 0.336$ (Fig. 9c). The heating then decreases from the center outward in sinusoidal form to zero at the boundaries in both the longitudinal and meridional directions. This perpetual July experiment is labeled LH-0P. The results shown in Fig. 9 demonstrate that over the heating region a southerly is forced at 850 hPa below the maximum heating (Fig. 9b), whereas a northerly is forced at 200 hPa above the maximum heating (Fig. 9a). Figure 9c shows the vertical cross section of the zonal deviation of geopotential height along 30°N where the initial U is about 4 m s^{-1}. Above the level of maximum heating, positive and negative geopotential heights are generated, respectively, to the west and east of the heating; whereas below this level, the pattern is out of phase with that in the upper layer. These are the results anticipated from the Sverdrup balance (1), which are in good agreement with the observations presented in Fig. 3. However, the anticyclone centers in both the upper and lower layers are too close to the heating (Fig. 9c) compared to observations. Comparison of Fig. 9c with Fig. 8c shows that over the heating region, the surface sensible heating tends to generate an out-of-phase vertical pattern of the geopotential height, whereas the deep convective heating tends to produce meridional winds in the free atmosphere subject to the Sverdrup relation (1) that was defined as a ''local mode'' by Chen (2001) and a surface cyclone in response to the heating. The main features presented in Fig. 9c are also captured in the analytical solutions of Chen based on a linear quasigeostrophic model (QG) and under a 5 m s^{-1} basic flow (his Fig. 7e). However, two significant differences exist between the GCM and the linear QG outputs. First, the linear advection in the QG moves the local mode eastward, resulting in a striking out-of-phase vertical structure in streamfunction above the heating region. On the contrary, in the GCM as shown in Fig. 9c, despite the existence in the initial fields of the basic westerly zonal flow (4 m s^{-1}) along 30°N, such a local mode is over the heating region, just like the resting basic flow solutions in Chen (his Fig. 7a). This is because in a

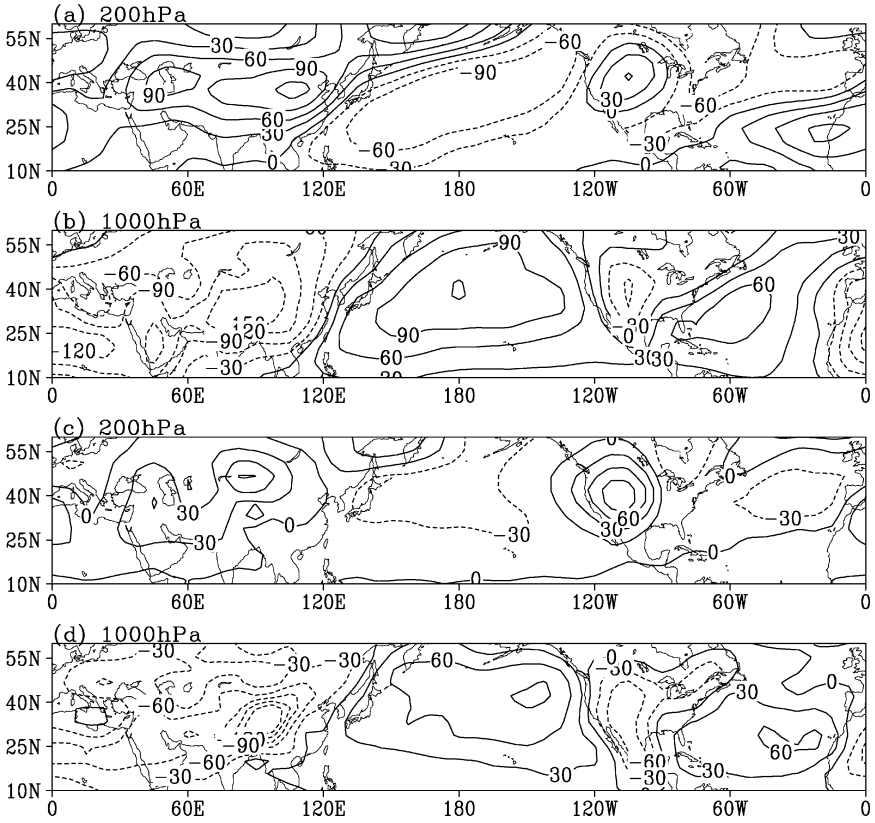

FIG. 10. Jul mean zonal deviations of geopotential height (units are gpm) at (a), (c) 200 and (b), (d) 1000 hPa calculated from the GCM experiments (a), (b) SH-1 and (c), (d) SH-2.

GCM, the strong subtropical CO heating along the weak zonal westerly basic flow can result in a strong westerly to the north and an easterly to the south of the heating region, and can produce a resting zonal flow across the heating region. Such a mechanism of the reaction of the basic flow to the heating is absent in the linear model, and the model solutions become very sensitive to the prescribed basic flow as was reported. Second, the maximum amplitudes of the streamfunction in the QG solutions appear near the top (14 km) and at the lower boundary of the heating (Figs. 5 and 7 in Chen). This is because the heating profile given as a function of sin (αz) with $\alpha = \pi/(14$ km) in his study produces a vorticity forcing proportional to cos (αz) that is maximized at the upper and lower boundaries. As a result a strong surface anticyclone is forced in the local mode. However, in the GCM, a strong subtropical anticyclone does not appear at the surface. Instead, the maximum amplitudes appear just to the west and east of the heating center at, respectively, $\sigma = 0.189$ and 0.500, one level above and below the maximum heating level ($\sigma = 0.336$). Due to the strong CO heating, the static stability close to the heating center becomes very small, and the vorticity forcing in the Sverdrup balance (1) is maximized just below and above the heating center. Such a mechanism of the heating-adjusted static stability and vorticity forcing is also absent in the prescribed forcing in the QG model, and the local mode in a resting basic flow exhibits an antisymmetric pattern about the heating center (Fig. 5a in Chen). We will show that the GCM results presented in LH-0P (Fig. 9) are more robust not only in the following experiments, but also in other studies based on different models.

b. Sensitivity experiments

1) SENSIBLE HEATING AND RADIATIVE COOLING

Two sensitivity experiments are designed. The first experiment is similar to CON but with the removal of surface sensible heating in the thermodynamic equation. The difference between CON and this first run then approximately represents the atmospheric response to surface sensible heating alone, and is labeled SH-1. The second experiment is also similar to CON but with the removal of latent heating in the thermodynamic equation. The results are labeled SH-2 and can be considered as the atmospheric response to surface sensible heating and radiative cooling (Table 1). The results from these two experiment sets are presented in Fig. 10. The distributions of the zonal deviation of geopotential height in SH-1 (Figs. 10a and 10b) agree in general with those

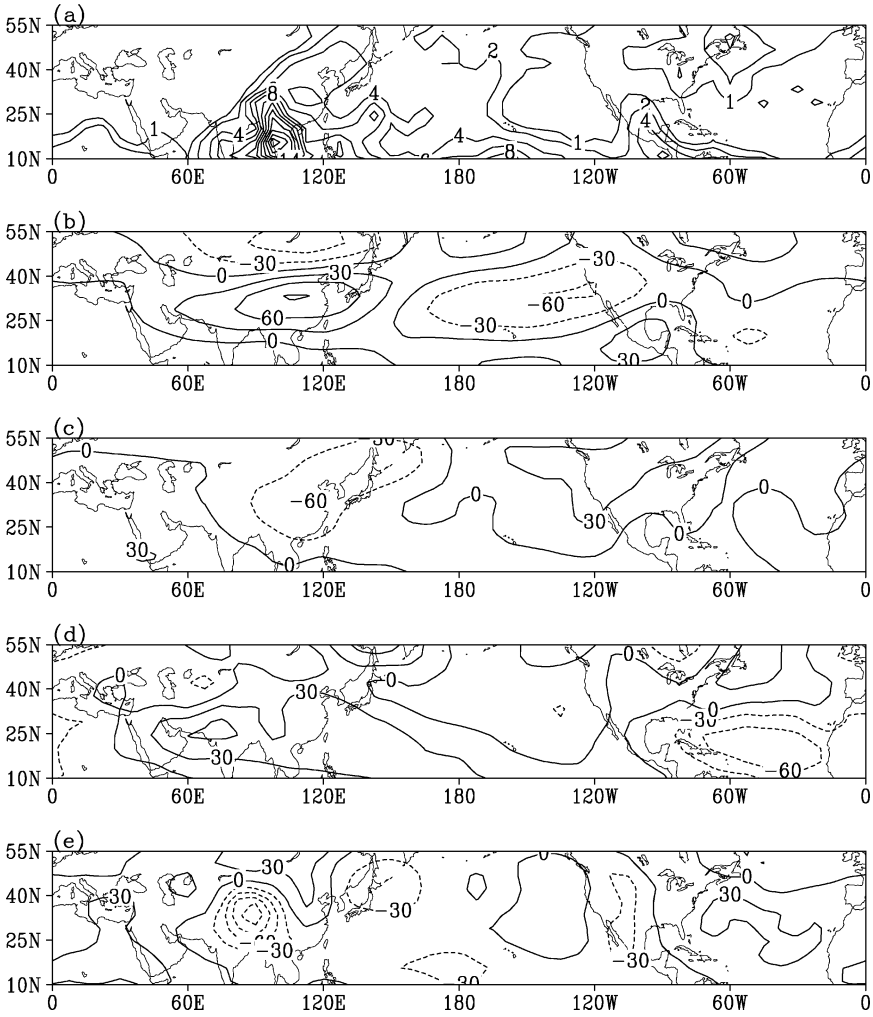

FIG. 11. (a) Jul mean precipitation in CON (units are mm day^{-1}), and the zonal deviations of geopotential height (units are gpm) at (b), (d) 200 and (c), (e) 1000 hPa calculated from the perpetual Jul experiments (b), (c) LH-1P and (d), (e) LH-2P.

in CON (Fig. 7), and the intensities of the upper- and lower-layer anticyclones are close to their counterparts in CON. These imply the significance of the surface sensible heating over land in the formation of the summertime subtropical circulations. However, the centers of the surface subtropical anticyclones and the upper-layer cyclones over the North Pacific and North Atlantic shift too far to the west compared to those in CON. In particular, the surface subtropical anticyclone over the North Pacific looks rather symmetric about the date line. These may be attributed to the lack of radiative cooling as was proposed in the preceding section. In SH-2 in which both the effects of the surface sensible heating and the radiative cooling are presented, the zonal asymmetry of these oceanic systems appears, and the simulated subtropical circulations (Figs. 10c and 10d) are closer to those in CON. The anticyclone center over the North Pacific is located at 145°W both in SH-2 and in CON, in agreement with the observation (Fig. 2d). Results from the above experiments then prove that it is mainly the radiative cooling over the eastern oceans that changes the symmetric surface anticyclones over the oceans to asymmetric, and shifts their centers eastward toward the western coasts of the continents. The main discrepancy between SH-2 and CON exists over the western oceans. This may be attributed to the exclusion of condensation impacts in SH-2.

2) CONDENSATION HEATING

The July mean rainfall distribution in CON is presented in Fig. 11a. It is close to the distribution of the condensation heating in the NCEP–NCAR reanalysis (Figs. 3c and 3d). To investigate the impacts of such a condensation heating on the circulation, a pair of the aforementioned perpetual July experiments is assigned. The first experiment, called LH-1P (Table 1), assumes an aquaplanet and uses the three-dimensional distribu-

tion of the condensation heating that exists in CON and is consistent with the rainfall distribution presented in Fig. 11a. The second experiment is the same as LH-1P but with the inclusion of orography and the replacement of the zonal mean SST by the observed SST, and defined as LH-2P (Table 1). Results from LH-1P are shown in Figs. 11b and 11c. In response to the latent heating from eastern China to the date line along the subtropics, the in situ surface southwesterlies and strong upper-layer northeasterlies appear. A strong upper-layer anticyclone is formed to the west of the heating, while the surface anticyclone is formed to its east, as expected from the Sverdrup balance (1). The strong rainfall over Latin America is accompanied by a surface low and an upper-layer high, respectively. It is worthwhile to compare these with the corresponding results of other studies. Using a linear two-layer model, Webster (1972) introduced a latent heating distribution for June–July–August (JJA) as a prescribed diabatic heating to the integration, which was based on the estimates of cloudiness and also possesses a maximum over China and the western Pacific along the boreal subtropics (his Fig. 2c). Strong northeasterlies at 250 hPa and southwesterlies at 750 hPa were generated over this heating area, and a strong upper-layer subtropical anticyclone from Japan to eastern North Africa and a weaker low-layer subtropical anticyclone over the western Pacific were produced (his Fig. 15). Similar features are also presented in the linear model outputs of Lin (1983, his Fig. 9). They agree well with those shown in Fig. 9 and Figs. 11b and 11c.

In all these experiments, the center of the upper-layer anticyclone is located over eastern China, too far to the east compared to the observation (Fig. 2c). This is in agreement with the results of LH-0P (Fig. 9), in which the center of the upper-layer anticyclone is just to the west of the heating center. In LH-2P, in which the orography distribution is included, the locations of both the surface cyclone and upper-layer anticyclone are shifted westward.

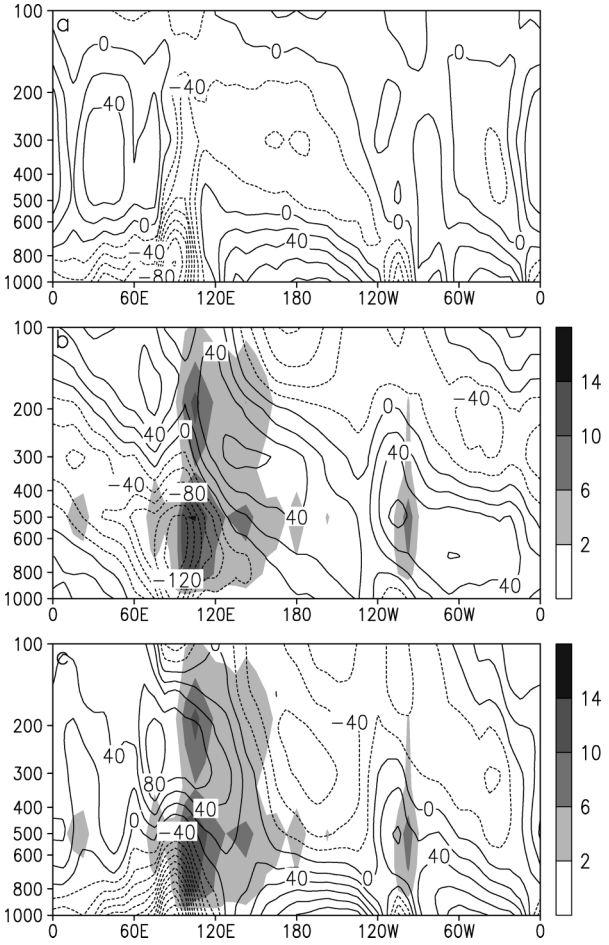

FIG. 12. Cross sections of the zonal deviation of geopotential height (units are gpm) along 30°N in perpetual Jul experiments (a) SH-2P, (b) LH-2P, and (c) CON-P. Shading indicates the Jul distribution of precipitation in CON, which is taken as a latent heating source in the experiment.

3) Comparison between sensible heating and condensation heating

For this purpose, another pair of perpetual July experiments is designed. The first is similar to LH-2P but with the inclusion of sensible heating, and labeled CON-P. The second is the same as CON-P but with the removal of the latent heating in the thermodynamic equation and labeled SH-2P (Table 1). The CON-P and SH-2P runs correspond to, respectively, the full GCM experiments CON and SH-2 described before except for the usage of the perpetual July setting. The distributions of the July mean geopotential height field in the perpetual runs are similar to those in the corresponding GCM experiments (figures not shown), and the usage of the perpetual July experiment for the present purpose is validated. The cross sections along 30°N of the zonal deviation of the geopotential height for these experiments are shown in Fig. 12. The vertical out-of-phase feature in SH-2P (Fig. 12a) is similar to that in the idealized experiment SH-0P (Fig. 8c), and enhanced due to the inclusion of orography. In LH-2P (Fig. 12b), the Sverdrup balance pattern that was obtained from the idealized run LH-0P (Fig. 9c) is prominent over either the Asian monsoon region or the North American monsoon region: the local maximum positive geopotential height is observed to the west of the maximum heating in the upper layer and to its east in the lower layer, not at the surface. In addition, a surface cyclone exists just below the heating.

It is interesting to compare the results of SH-2P and LH-2P with those of CON-P. The vertical out-of-phase feature in CON-P is well simulated in SH-2P particularly over the oceans. Surface continental cyclones and oceanic anticyclones in CON-P are also presented well in SH-2P. The magnitude of the surface anticyclone over the Pacific in SH-2P is over 80 gpm and accounts for about 80% of its counterpart in CON-P (>100 gpm),

and that over the Atlantic is more than 60 gpm and accounts for more than 70% of its counterpart in CON-P (>80 gpm). The contributions to these surface anticyclones from condensation heating become secondary. In these aspects, sensible heating is more important than latent heating in maintaining the circulations. Over the two monsoon regions, however, the geopotential height fields in CON-P bear the strong impacts of the Sverdrup balance, which is driven by condensation heating. As a result, a geopotential height center of 60 gpm at 200 hPa over Asia and another center of similar strength at 500 hPa over North America produced by condensation heating in LH-2P are rather close to their counterparts in CON-P, and the subtropical anticyclone at 500 hPa over western Pacific in CON-P owes its existence mainly to the condensation heating. It is important to note that the sensible heating and condensation heating act together to strengthen the anticyclone over Asia and the troughs over oceans in the upper troposphere, as well as the oceanic subtropical anticyclones and the huge Asian cyclone near the surface.

It becomes clear that the sensible heating and condensation heating in summer play different roles in maintaining the subtropical circulations. Together with radiative cooling, they are all important in forming the summertime subtropical anticyclones. Although the magnitude of the latent heating associated with the summer monsoon is stronger than the sensible heating, the sensible heating over the land surface is more fundamental in maintaining the summertime subtropical anticyclones near the surface. It also contributes significantly to the vertical out-of-phase features of the subtropical circulation.

The above conclusion contradicts those drawn by Webster (1972) and Egger (1978), who attempted to separate the contributions of sensible and latent heating to the maintenance of the summertime subtropical anticyclones and stressed the dominant importance of latent heating. However, as shown in Fig. 5, a substantial part of sensible heating is concentrated below 800 hPa. Such very low-layer heating exerts profound impacts on the circulations not only in the lower layers but also in the upper layers as demonstrated in Figs. 8, 10, and 12. However, the sensible heating above 800 hPa is negligible compared with other heating over all heating lobes (Fig. 5). Therefore it may not be appropriate to evaluate the impacts of sensible heating on the atmospheric circulation by only using the kinds of two-layer circulation models in which the lower layer is at either 800 or 750 hPa. Chen et al. (2001) introduced two latent heating sources, respectively, over Asia and North America to the aforementioned linear QG model (Chen 2001) to study the atmospheric responses to the summertime diabatic heating, and interpreted the surface oceanic subtropical anticyclones in the Northern Hemisphere as a remote response of Rossby waves forced by the large-scale heating source over Asia, and the circulations over the two continents as a local response to monsoon latent heat release in the midtroposphere. As discussed before, the lack of the mechanism in the QG model of the heating-adjusted static stability and vorticity forcing can lead to an exaggerated surface response. In addition, the observed monsoon rainfall is located from eastern China to the western Pacific and from eastern North America to the western Atlantic (Fig. 3), whereas the imposed latent heating sources for their experiment were located between 50° and 130°E and between 116° and 94°W, too far to the west of the observations. These differences make it difficult to compare the current study with their results.

5. Synthetic thermal forcing and distribution of the subtropical anticyclone

The above analysis implies that the land–sea distribution in the summer subtropics is crucial in forming the distributions of the subtropical anticyclone, and the roles of the different kinds of diabatic heating across each continent and its adjacent oceans should be considered synthetically. To verify this further, the distributions of the circulation pattern against the local dominant thermal forcing along the subtropics are presented in Fig. 13 based, again, on the NCEP–NCAR reanalysis. The subtropical area in the two hemispheres is divided into five subareas, each having one continent located at its center. The distributions of the local dominant heating/cooling are presented in Figs. 13a and 13d. Those SEs stronger than 30 W m^{-2} are shaded in orange and red, and COs stronger than 50 W m^{-2} are in green. Because the radiative cooling over oceans is very strong, only those LO stronger than -220 W m^{-2} are shown in blue so that the secondary dominant heating (CO) over the western oceans can be presented. For the purposes of comparison, the labels L, S, C, and D marked in Fig. 1b are also marked in Fig. 13. Following Wu and Liu (2003), the labels L, S, C, and D are located, respectively, in the lobes over which the LO, SE, CO, and D heatings prevail (Fig. 5). The LOSECOD heating quadruplet is observed over each subarea, although its zonal scale varies from one subarea to another. In coordination with each heating quadruplet, the circulations in the upper troposphere (Figs. 13b and 13e) and in the lower troposphere (Figs. 13c and 13f) exhibit a specific pattern: the surface cyclone and upper-layer anticyclone are located over the SE and CO lobes over the continent, with the surface cyclone accompanied with anticyclonic circulations on its western and eastern sides over oceans, and the upper-layer anticyclone accompanied with cyclonic circulations on the both sides over oceans. Because the amplitude of the forced circulation depends on the horizontal scale and intensity of the forcing, in response to the larger-scale SE and CO lobes over Asia the upper-layer Asian anticyclone is much stronger than its counterparts over other continents. In addition, in response to the decrease/increase with height of the dominant heating in the lower/upper layers, the strong

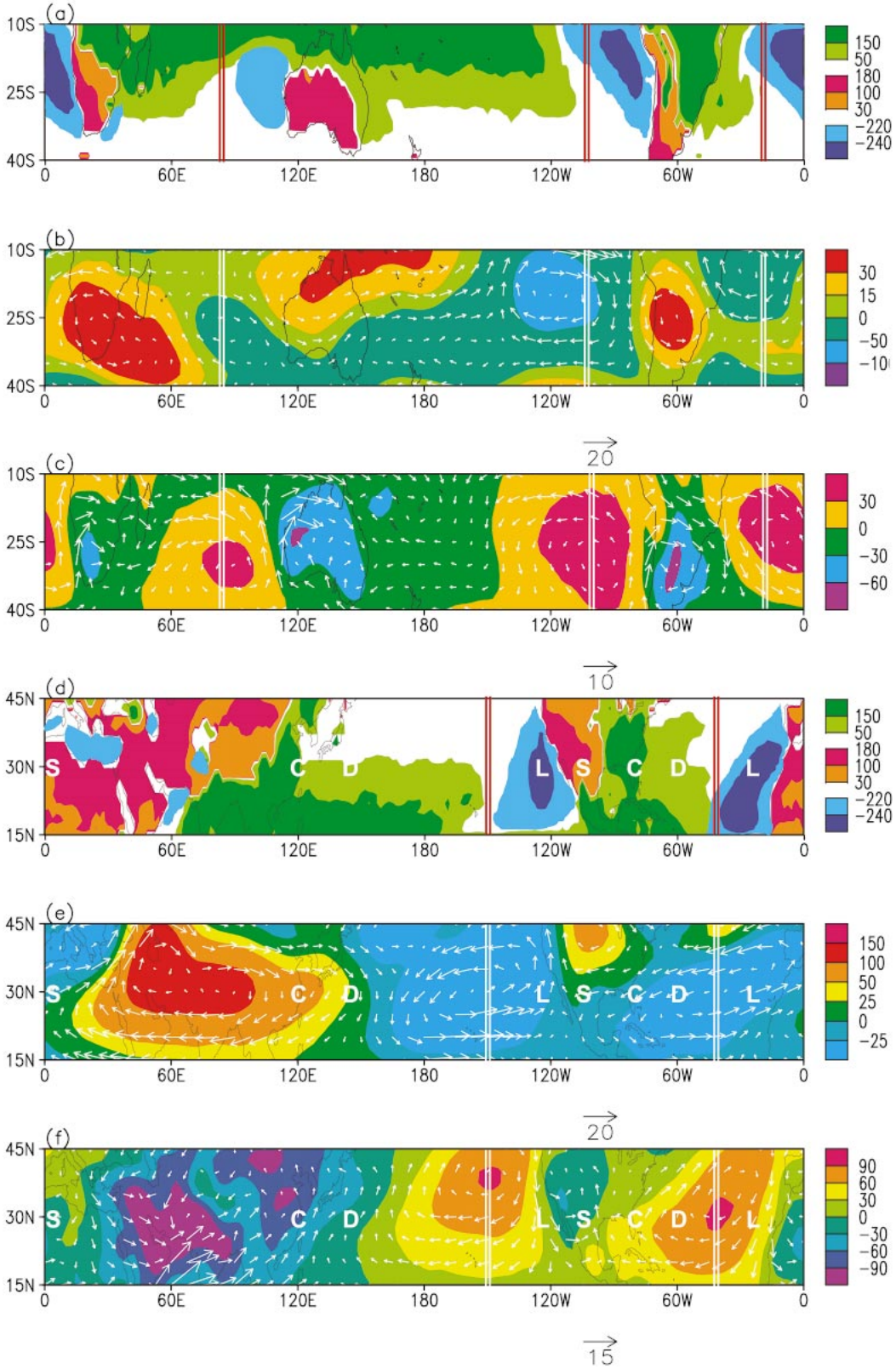

FIG. 13. Distributions in (a)–(c) Jan in the southern subtropics and (d)–(f) Jul in the northern subtropics of the (a), (d) different kinds of dominant heating with units of W m^{-2}, and the zonal deviations of wind (arrow) and geopotential height (shaded) at (b), (e) 200 and (c), (f) 1000 hPa with units of gpm. The sites L, S, C, and D as shown in Fig. 1b indicate, respectively, the locations in the LO, SE, CO, and D heating lobes.

surface equatorward flow and upper-layer poleward flow are found over the LO and SE lobes in the west. Whereas in response to the increase/decrease with height of the dominant heating in the lower/upper layers, the surface poleward flow and stronger upper-layer equatorward flow are observed over the CO and D lobes in the east. The circulation pattern, therefore, presents a zonally asymmetric configuration. Furthermore, when the circulation patterns over the five subareas are tiled side-by-side, the lower-layer oceanic subtropical anticyclone and the upper-layer trough appear at the edges of the two adjacent subareas, whereas the upper-layer continental subtropical anticyclone and lower-layer cyclone appear at the center of each subarea. Therefore the global general circulation in the summer subtropics can be viewed as a mosaic of the unique circulation pattern over each subarea.

6. Conclusions and discussion

It has been shown that the atmospheric thermal adaptation to the sensible and condensation heating over land and radiative cooling over ocean are essential in producing subtropical anticyclones over continents in the upper troposphere and over oceans in the lower troposphere. The surface sensible heating over the land surface is fundamental in maintaining the summertime subtropical anticyclones near the surface. It also contributes significantly to the vertical out-of-phase features of the subtropical circulation. Because the isentropic surfaces in the subtropics in the lower-troposphere slope upward toward higher latitudes, adiabatic flows slide downward on the eastern side of the lower-tropospheric anticyclone, but upward on its western side. Because the horizontal advection of vorticity is neglectable along the anticyclonic ridgeline, the atmospheric vertical motion there is mainly determined by the vertical shear of the meridional winds at a steady state. Therefore the thermally adapted meridional flows cause descending motion over the eastern ocean and western continent, and ascending motion over the western ocean and eastern continent, just in phase with the adiabatic ascent/descent.

As pointed out by Rodwell and Hoskins (2001), the descending motion over the eastern ocean increases the air temperature and reduces its relative humidity above the cold ocean surface, stabilizing the air and forming low stratus clouds in the planetary boundary layer, in favor of the in situ radiative cooling near the top of the planetary boundary layer and the development of diabatic descending motion. On the other hand, the ascent over the western ocean decreases the air temperature and increases its relative humidity, in favor of the development of convection and diabatic ascent. The maximum radiative cooling over the eastern ocean occurs below the level $\sigma = 0.8$, and the maximum condensation heating over the western ocean occurs near $\sigma = 0.3$ (Fig. 5). Following the Sverdrup balance (1), stronger equatorward flow and anticyclone vorticity are produced on the eastern sides of the surface anticyclone over oceans and the upper-layer anticyclone over continents, whereas weaker poleward flow and cyclone vorticity are produced on the eastern sides of the upper-layer troughs over oceans and the surface cyclones over continents. Such asymmetric meridional winds induced by condensation heating and radiative cooling then strengthen the circulation pattern along the subtropics, which was produced by the sensible heating over land, and deform its configuration both in the upper and lower troposphere. Surface anticyclone centers are shifted eastward, whereas the upper-tropospheric troughs tilt from the east in high latitudes to the west in low latitudes. The pattern of asymmetric subtropical circulation is then formed. Therefore, we can reach the conclusion that different types of heating play different roles and all are important in the formation of the summertime subtropical anticyclones. Their maintenance is closely associated with the land–sea distribution and can be interpreted in terms of the atmospheric adaptation to diabatic heating by using the PV–θ view and the Sverdrup balance (1). The global summer subtropical heating and circulation may be viewed as ''mosaics'' of the LOSECOD heating quadruplet and circulation patterns, respectively.

Although the primary relation between diabatic heating and the formation of the subtropical anticyclone has been investigated in this study, many questions still remain unclear or have been left untouched. For instance, how does a unique heating quadruplet exist over each continent area in summer? Why are the radiative cooling and vertical descending motion so strong and so well coupled over the eastern oceans? What is the role of air–sea interaction in this coupling? Besides these, some more practical problems concern the variability of the subtropical anticyclone at synoptic scales. In such circumstances, not only external forcing, but also internal forcing, including the interaction of circulations in different latitudes and between different weather systems, are both important. All these problems are significant for further understanding the nature and variations of the subtropical anticyclones and need to be investigated. We look forward to seeing more new insights on these points in the near future.

Acknowledgments. This study was supported jointly by the Chinese Academy of Sciences under Project ZKCX2-SW-210 and the National Excellent Ph.D. Thesis Award, and by the Natural Science Foundation of China under Projects 40135020, 40023001, and 40221503.

REFERENCES

Bolin, B., 1950: On the influence of the earth's orography on the westerlies. *Tellus,* **2,** 184–195.

Charney, J. G., and A. Eliassen, 1949: A numerical method for predicting the perturbations of the middle latitude westerlies. *Tellus,* **1,** 38–54.

Chen, P., 2001: Thermally forced stationary waves in a quasigeostrophic system. *J. Atmos. Sci.,* **58,** 1585–1594.
——, M. P. Hoerling, and R. M. Dole, 2001: The origin of the subtropical anticyclones. *J. Atmos. Sci.,* **58,** 1827–1835.
Egger, J., 1978: On the theory of planetary standing waves: July. *Beitr. Phys. Atmos.,* **51,** 1–14.
Gill, A. E., 1980: Some simple solutions for heat-induced tropical circulation. *Quart. J. Roy. Meteor. Soc.,* **106,** 447–662.
Hoskins, B. J., 1987: Diagnosis of forced and free variability in the atmosphere. *Atmospheric and Oceanic Variability*, H. Cattle, Ed., James Glaisher House, 57–73.
——, 1991: Towards a PV–θ view of the general circulation. *Tellus,* **43AB,** 27–35.
——, 1996: On the existence and strength of the summer subtropical anticyclones. *Bull. Amer. Meteor. Soc.,* **77,** 1287–1292.
Houghton, J. T., Y. Ding, D. J. Griggs, M. Noguer, P. J. van der Linden, and D. Xiaosu, Eds., 2001: Model evaluation. *Climate Change 2001: The Scientific Basis. Contribution of Working Group I to the Third Assessment Report of the Intergovernmental Panel on Climate Change,* Cambridge University Press, 471–523.
Kalnay, E., and Coauthors, 1996: The NCEP/NCAR 40-Year Reanalysis Project. *Bull. Amer. Meteor. Soc.,* **77,** 437–471.
Kang, I.-S., and Coauthors, 2002: Intercomparison of atmospheric GCM simulated anomalies associated with the 1997/98 El Niño. *J. Climate,* **15,** 2791–2805.
Li, G. P., T. Y. Duan, and S. Haginoya, 2001: Estimates of the bulk transfer coefficients and surface fluxes over the Tibetan Plateau using AWS data. *J. Meteor. Soc. Japan,* **79,** 625–635.
Lin, B.-D., 1983: The behavior of stationary waves and the summer monsoon. *J. Atmos. Sci.,* **40,** 1163–1177.
Lin, X., and R. H. Johnson, 1996: Heating, moistening, and rainfall over the western Pacific warm pool during TOGA COARE. *J. Atmos. Sci.,* **53,** 3367–3383.
Liu, H. and G. X. Wu, 1997: Impacts of land surface on climate of July and onset of summer monsoon: A study with an AGCM plus SSiB. *Adv. Atmos. Sci.,* **14,** 289–308.
Liu, Y. M., H. Liu, P. Liu, and G. X. Wu, 1999a: Spatially inhomogeneous diabatic heating and its impacts on the formation and variation of subtropical anticyclone. II. Land-surface sensible heating and the subtropical anticyclone over the northeast Pacific and North America. *Acta Meteor. Sin.,* **57,** 385–396.
——, G. X. Wu, H. Liu, and P. Liu, 1999b: Spatially inhomogeneous diabatic heating and its impacts on the formation and variation of subtropical anticyclone. III. Convective condensation heating and the subtropical anticyclone over south Asia and northwest Pacific. *Acta Meteor. Sin.,* **57,** 525–538.
——, ——, ——, and ——, 2001: Dynamical effects of condensation heating on the subtropical anticyclones in the Eastern Hemisphere. *Climate Dyn.,* **17,** 327–338.
Newman, M., P. D. Sardeshmukh, and J. W. Bergman, 2000: An assessment of the NCEP, NASA, and ECMWF reanalyses over the tropical west Pacific warm pool. *Bull. Amer. Meteor. Soc.,* **81,** 41–48.
Nigam S., C. Chung, and E. DeWeaver, 2000: ENSO diabatic heating in ECMWF and NCEP–NCAR reanalyses, and NCAR CCM3 simulation. *J. Climate,* **13,** 3152–3171.
Rodwell, M. R., and B. J. Hoskins, 2001: Subtropical anticyclones and monsoons. *J. Climate,* **14,** 3192–3211.
Webster, P. J., 1972: Response of the tropical atmosphere to local, steady forcing. *Mon. Wea. Rev.,* **100,** 518–541.
Wu, G. X., and Y. M. Liu, 2000: Thermal adaptation, overshooting, dispersion and subtropical anticyclone. I. Thermal adaptation and overshooting. *Chin. J. Atmos.,* **24,** 433–446.
——, and ——, 2003: Summertime quadruplet heating pattern in the subtropics and the associated atmospheric circulation. *Geophys. Res. Lett.,* **30**, 1201, doi:10.1029/2002GL016209.
——, W. P. Li, H. Guo, H. Liu, J. S. Xue, and Z. Z. Wang, 1997a: The sensible heat driven air-pump over the Tibetan Plateau and the Asian summer monsoon. *Collection in the Memory of Dr. Zhao Jiuzhang*, D. Ye, Ed., Chinese Science Press, 116–126.
——, and Coauthors, 1997b: The LASG global ocean–atmosphere–land system model GOALS/LASG and its simulation study. *Appl. Meteor.,* **8** (special issue), 15–28.
——, Y. M. Liu, and P. Liu, 1999: Spatially inhomogeneous diabatic heating and its impacts on the formation and variation of subtropical anticyclone. I. Scale analysis. *Acta Meteor. Sin.,* **57,** 257–263.
Xue, Y. K., P. J. Sellers, J. L. Kinter, and J. Shukla, 1991: A simplified biosphere model for global climate studies. *J. Climate,* **4,** 345–364.
Ye, D. Z., and G. X. Wu, 1998: The role of the heat source of the Tibetan Plateau in the general circulation. *Meteor. Atmos. Phys.,* **67,** 181–198.
Yeh, T. C., 1950: The circulation of the high troposphere over China in the winter of 1945–1946. *Tellus,* **2,** 173–183.
Zhang, X. H., and Coauthors, 1996: Simulation of thermohaline circulation with a twenty-layer oceanic general circulation model. *Theor. Appl. Climatol.,* **55,** 65–88.
——, G. Y. Shi, H. Liu, and Y. Q. Yu, 2000: *IAP Global Ocean-Atmosphere-Land System Model.* Science Press, 252 pp.